Reprinted from

JAPANESE JOURNAL OF
APPLIED
PHYSICS

REGULAR PAPER

Automated Identification of the Heart Wall Throughout the Entire Cardiac Cycle Using Optimal Cardiac Phase for Extracted Features

Hiroki Takahashi, Hideyuki Hasegawa, and Hiroshi Kanai

Jpn. J. Appl. Phys. **50** (2011) 07HF16

Japanese Journal of Applied Physics **50** (2011) 07HF16 **REGULAR PAPER**
DOI: 10.1143/JJAP.50.07HF16

Automated Identification of the Heart Wall Throughout the Entire Cardiac Cycle Using Optimal Cardiac Phase for Extracted Features

Hiroki Takahashi[1], Hideyuki Hasegawa[1,2], and Hiroshi Kanai[1,2]*

[1]*Graduate School of Biomedical Engineering, Tohoku University, Sendai 980-8579, Japan*
[2]*Graduate School of Engineering, Tohoku University, Sendai 980-8579, Japan*

Received December 13, 2010; accepted February 7, 2011; published online July 20, 2011

In most methods for evaluation of cardiac function based on echocardiography, the heart wall is currently identified manually by an operator. However, this task is very time-consuming and suffers from inter- and intraobserver variability. The present paper proposes a method that uses multiple features of ultrasonic echo signals for automated identification of the heart wall region throughout an entire cardiac cycle. In addition, the optimal cardiac phase to select a frame of interest, i.e., the frame for the initiation of tracking, was determined. The heart wall region at the frame of interest in this cardiac phase was identified by the expectation–maximization (EM) algorithm, and heart wall regions in the following frames were identified by tracking each point classified in the initial frame as the heart wall region using the *phased tracking method*. The results for two subjects indicate the feasibility of the proposed method in the longitudinal axis view of the heart.

1. Introduction

In conventional echocardiography, structural change and macroscopic motion of the heart are diagnosed by measuring cross-sectional images, and quantitative evaluation of intracardiac blood flow and cardiac wall motion can also be performed by ultrasound Doppler measurements.[1,2] Moreover, various valuable methods for evaluation of cardiac function based on echocardiography, such as evaluation of two-dimensional cardiac wall motion and strain rate by the speckle tracking method,[3–6] measurement of the propagation of vibration caused by the closure of valves,[7] and measurement of the transient of myocardial contraction and relaxation for about 10 ms,[8,9] have been developed. In most of the above-mentioned methods, the heart wall, which is the object to be analyzed, is currently identified manually by an operator. However, this task is very time-consuming and suffers from inter- and intraobserver variability.[10–12] For elimination of operator dependence and facilitation of analysis, automated identification of the heart wall is essential.

Various studies on segmenting regions in ultrasonic images have been conducted. Papadogiorgaki *et al.* proposed techniques for automated detection of lumen and media–adventitia borders for intravascular ultrasonography (IVUS).[13] Chang *et al.* classified the thyroid gland and directly estimated its volume in ultrasonic images.[14] In the cited studies, objects in an ultrasonic image are segmented using features extracted from the magnitude of the received ultrasonic signal. Furthermore, Torp *et al.* proposed a method for automatic detection of several candidate points in the apical view of the left ventricle.[15] This method also extracts features from the gray-scale value, the velocity, and the depth to detect the candidate points. The object of interest, i.e., the heart wall, can be identified automatically based on features and can be identified manually using observable features such as brightness and macroscopic motion in an ultrasonic image. Therefore, the extraction of valid features from acquired ultrasonic images (or signals) is important for the identification of objects of interest.

Nillesen *et al.* introduced a method in which echogenicity was smoothed in each local area to distinguish the heart wall from lumen.[16] However, the method using only echogenicity would misclassify a region with a low echogenicity inside the heart wall as lumen. To overcome this limitation, Kinugawa *et al.* proposed a method of identification of the heart wall using coherence between echoes.[17] However, the separability of this method is degraded by a stationary component owing to echoes from external tissue such as ribs because this component increases the coherence of echoes from the heart wall and lumen. The present paper introduces multiple features to reduce the influences of such undesirable echo characteristics, which would degrade the accuracy of the identification of the heart wall.

Segmentation of the ventricular endocardial surface in each frame in an echocardiographic image sequence during one cardiac cycle is made possible by tracking the position of the endocardial surface determined at a certain frame[12] using one-dimensional (1D) or two-dimensional (2D) tracking methods. In the present study, the heart wall region at a frame of interest (the frame where tracking is initiated) was identified automatically by classification using multiple features extracted from echo signals, which are measured at a high frame rate. Furthermore, to select the frame of interest, we identified the optimal cardiac phase for classification by multiple features.

2. Principles

2.1 Feature extraction

Figure 1(a) illustrates a plane in the heart, which was scanned by an ultrasound beam. With respect to each scan line position j, as shown in Fig. 1(b), ultrasonic RF echo signals scattered by the heart wall [e.g., interventricular septum (IVS) and left ventricular posterior wall (LVPW)] and lumen [e.g., right ventricle (RV) and left ventricle (LV)] are received with a time interval corresponding to the inverse of a frame rate.

Just like in conventional methods for segmentation of echocardiographic images, the magnitude of the echo signal was used as the first feature in the present study. The envelope-detected signal $Env(x;n)$, at a depth of x in the n-th frame, is extracted from the received ultrasonic RF echo signal $s(x;n)$ as follows:

$$Env(x;n) = \log_{10}[\mathrm{LPF}[(s(x;n))^2]], \quad (1)$$

where LPF[·] shows low-pass filtering with a cutoff frequency of 0.3 MHz (the transmit frequency of 3.75 MHz).

*E-mail address: kanai@ecei.tohoku.ac.jp

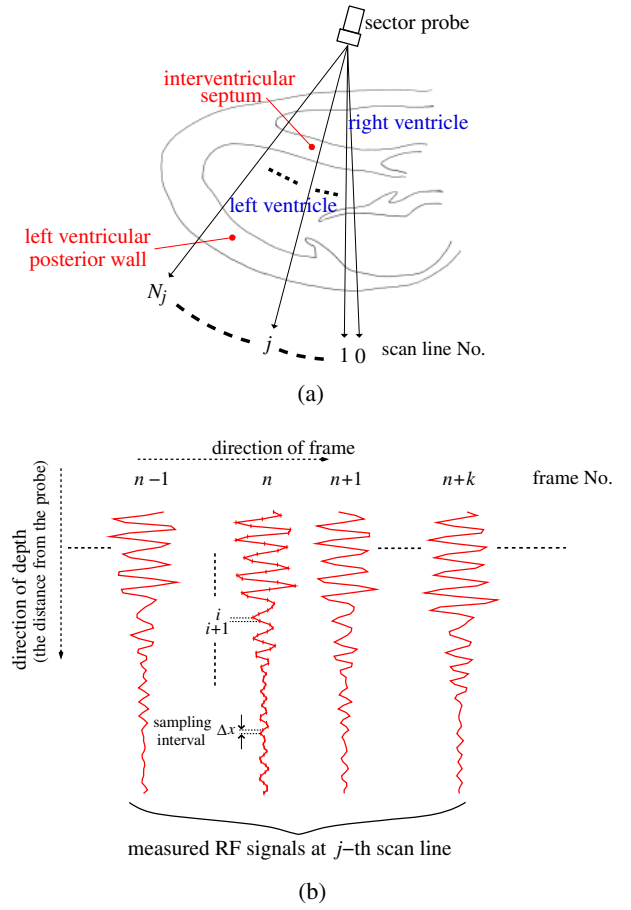

Fig. 1. (Color online) (a) Geometry of measurement by transthoracic echocardiography. (b) Illustration of variables of RF signals.

Nillesen *et al.* reduced the overlap between gray levels, corresponding to the magnitude of the backscattered signals, in the heart wall and lumen from 35.4 to 19.6% by smoothing in each local kernel for segmentation of the heart muscle in echocardiographic images.[16] However, using such methods, which depend only on the amplitude of the RF echo, the heart wall is not completely distinguished from the lumen because there is a region with a low echo level inside the heart wall. Hete and Shung found that the magnitude of the ultrasonic backscattered signals was changed by the orientation of muscle collagen fibers.[18] Wickline *et al.* suggested that the magnitude of ultrasonic backscatter is determined by local differences in acoustic impedance, which are affected by myocardial contraction and relaxation.[19] Thus, additional second and third features were adopted in this study to evaluate differences between echo signals of the heart wall and lumen regardless of the amplitude of backscattered signals as described below. In the ultrasonic RF signal measured at a high frame rate, the cardiac muscles in the heart wall can be tracked accurately by the *phased tracking method*.[20] As shown in Fig. 2, the temporal changes of waveforms of RF echo signals in a region of interest (ROI) placed in the heart wall region are fairly constant and can be tracked because the myocardium in the ROI stays in the focal area of the ultrasonic beam in two consecutive frames. On the other hand, blood cells in the cardiac lumen are difficult to track because they slip off from the focal area of the ultrasonic beam owing to blood flow. Therefore, the temporal change in the waveform of an ultrasonic echo in an ROI assigned in the lumen is significant. The displacement $u_x(n+k)$ between the n-th and $(n+k)$-th frames of tissue in an ROI assigned around depth x in the n-th frame is estimated by the *phased tracking method*, and complex spectra, $Y(f;\hat{x}(n+k);n+k)$ and $Y(f;\hat{x}(n+k+1);n+k+1)$, of RF signals in the ROIs at the positions, $\hat{x}(n+k)$ $[=x+u_x(n+k)]$ and $\hat{x}(n+k+1)$ $[=x+u_x(n+k+1)]$, in the $(n+k)$-th frame and $(n+k+1)$-th frame are obtained by applying the discrete Fourier transform (DFT) to RF signals in the ROIs. Using the complex spectra $\{Y(f;\hat{x}(n+k);n+k)\}$, the characteristics of phase changes of echoes in the ROI between two consecutive frames, which depends on the motion of an object, are evaluated by the magnitude-squared coherence (MSC) function[17,21] $|\gamma(f;x;n)|^2$ as follows:

$$|\gamma(f;x;n)|^2 = \frac{|\mathrm{E}_k[Y^*(f;\hat{x}(n+k);n+k)Y(f;\hat{x}(n+k+1);n+k+1)]|^2}{\mathrm{E}_k[|Y(f;\hat{x}(n+k);n+k)|^2]\mathrm{E}_k[|Y(f;\hat{x}(n+k+1);n+k+1)|^2]}, \quad (2)$$

where $\mathrm{E}_k[\cdot]$ and * denote the time averaging (for 50 frames) and complex conjugate, respectively. The numerator of eq. (2) denotes the absolute value of the mean of the complex cross spectra. Therefore, the consistency of the temporal changes in phases of complex spectra between two frames significantly affects this averaging operation shown in the numerator of eq. (2). Thus, eq. (2) evaluates the temporal variance in changes in the complex spectra of RF signals in the ROI between two consecutive frames.[17] Kinugawa *et al.* reported that the variance in the phase changes in the lumen shows relatively large values compared with that of the heart wall in the high frequency range.[17] In this study, the MSC at a frequency of 4.4 MHz, which was higher than the transmit frequency of 3.75 MHz, was used as the second feature.

As the third feature, the temporal mean of the changes in phases of RF signals between two consecutive frames was adopted because it cannot be evaluated by the MSC. The phase shift corresponds to the axial velocity of tissue and is obtained using the complex correlation technique.[22] Hatle and Angelsen showed that the peak blood velocity during systole of the left ventricle ranges from 0.7 to 1.1 m/s, while that during diastole of the left ventricle ranges from 0.6 to 1.3 m/s using the ultrasonic Doppler method.[23] The absolute value of the peak of myocardial velocities (IVS and LVPW), which were measured by Kapusta *et al.* using tissue Doppler imaging, was up to 0.2 m/s.[24] In this study, the phase shift due to the axial motion of tissue was extracted by estimation based on correlation of analytic signals $\{y_a(x;n)\}$ of RF signals $\{s(x;n)\}$, where analytic signals $\{y_a(x;n)\}$ were obtained by applying the quadrature demodulation to RF signals. The complex correlation function, $C(x;n)$, is calculated as follows:

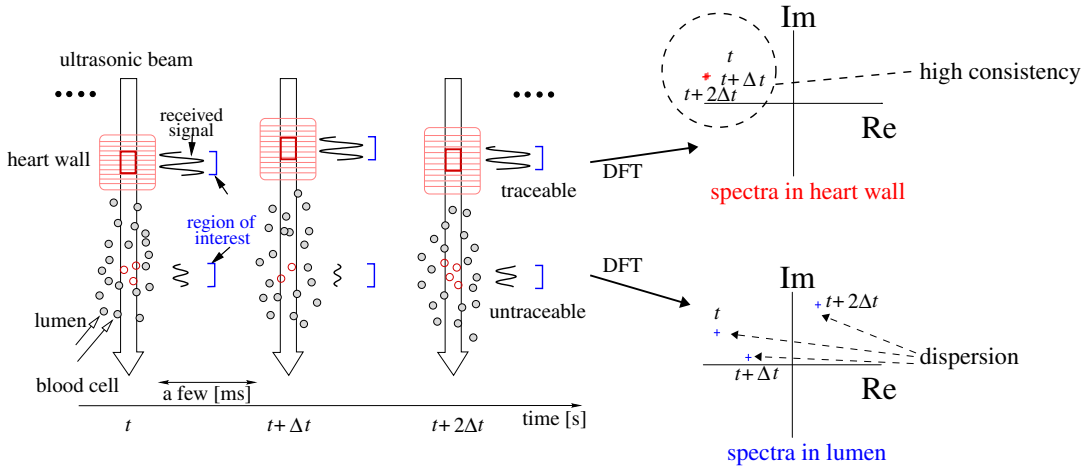

Fig. 2. (Color online) Illustration of changes of waveforms of echo signals in ROI.

$$C(x;n) = \frac{\sum_{k=-M_t}^{M_t-1} y_a^*(x;n+k)\cdot y_a(x;n+k+1)}{\sqrt{\sum_{k=-M_t}^{M_t-1}|y_a(x;n+k)|^2}\sqrt{\sum_{k=-M_t}^{M_t-1}|y_a(x;n+k+1)|^2}}, \quad (3)$$

where $2M_t$ determines the number of frames used for calculation of the correlation function and is set at 10 in the present study. The absolute value of the phase shift, $|\Delta\theta(x;n)|$, which is obtained by spatially averaging the estimator of eq. (3), was used as the third feature as follows:

$$|\Delta\theta(x;n)| = \left| < \left(\sum_{m=-M_d}^{M_d-1} C(x+m\Delta x;n) \right) \right|, \quad (4)$$

where Δx and $2M_d$ are the interval of the sampled signal in the axial direction and the number of sampled points used for spatial averaging ($2M_d \cdot \Delta x$ corresponds to a pulse duration defined by the width at -20 dB of the envelope of an ultrasonic pulse, about 1.44 mm).

By replacing x with the sampled point number i ($\equiv i \cdot \Delta x$) in the direction of depth and using the scan line number j, the envelope-detected signal $Env(x;n)$, the MSC $|\gamma(f;x;n)|^2$ at 4.4 MHz, and the absolute value of the phase shift $|\Delta\theta(x;n)|$ at the frame of interest are redefined as $Env(i,j)$, $|\gamma(i,j)|^2$, and $|\Delta\theta(i,j)|$, respectively.

Kinugawa *et al.* proposed a method for the identification of the heart wall using only MSC as the feature.[17] However, the MSC of echoes from the heart wall and lumen are sensitively increased by a stationary component owing to echoes from the ribs. In this study, therefore, the multiple features (e.g., the amplitude and the phase change of ultrasonic RF signals) were extracted from ultrasound echoes to overcome such problems, e.g., a low echogenicity inside the heart wall and a stationary component owing to echoes mainly from the ribs.

2.2 Enhancement of accuracy of features by filtering

The MSC of RF signals, the second feature, is increased owing to the components of echoes from external tissue such as the ribs[17] contained in the received RF signals. In addition, there is a considerable difference between the acoustic impedances of a rib and soft biological tissue. Therefore, the amplitude of the echo signal, the first feature, backscattered particularly from a shallow region in the heart, also becomes higher because it contains echoes from the ribs. Thus, reduction of the stationary components from the external tissue is necessary to accurately extract the features of the heart wall and lumen. In this study, to reduce this component, a third-order Butterworth high-pass filter[25] was used for the moving target indicator (MTI) filtering[26] of RF signals before calculating the first and second features, $Env(i,j)$ and $|\gamma(i,j)|^2$. Figure 3 shows the spatially averaged power spectrum distribution obtained by applying DFT with

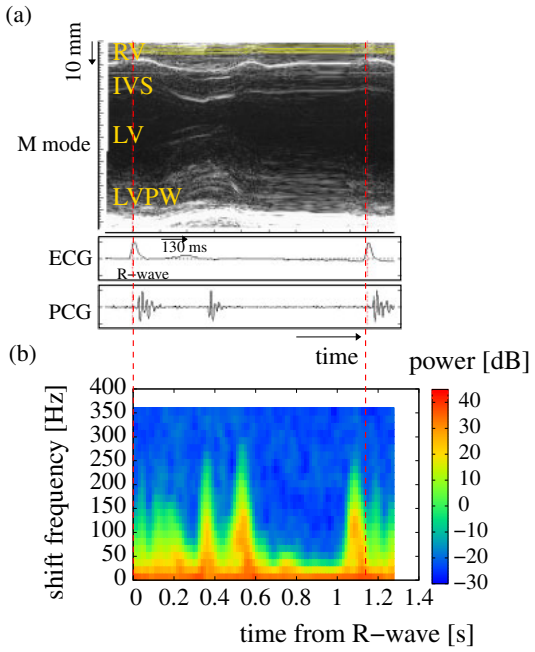

Fig. 3. (Color online) (a) M-mode image (RV: right ventricle, IVS: interventricular septum, LV: left ventricle, LVPW: left ventricular posterior wall). Yellow lines show tracking positions. (b) Spatial averaged power spectrum distribution obtained by applying DFT in the direction of frame (50 frames) to the yellow lines shown in (a).

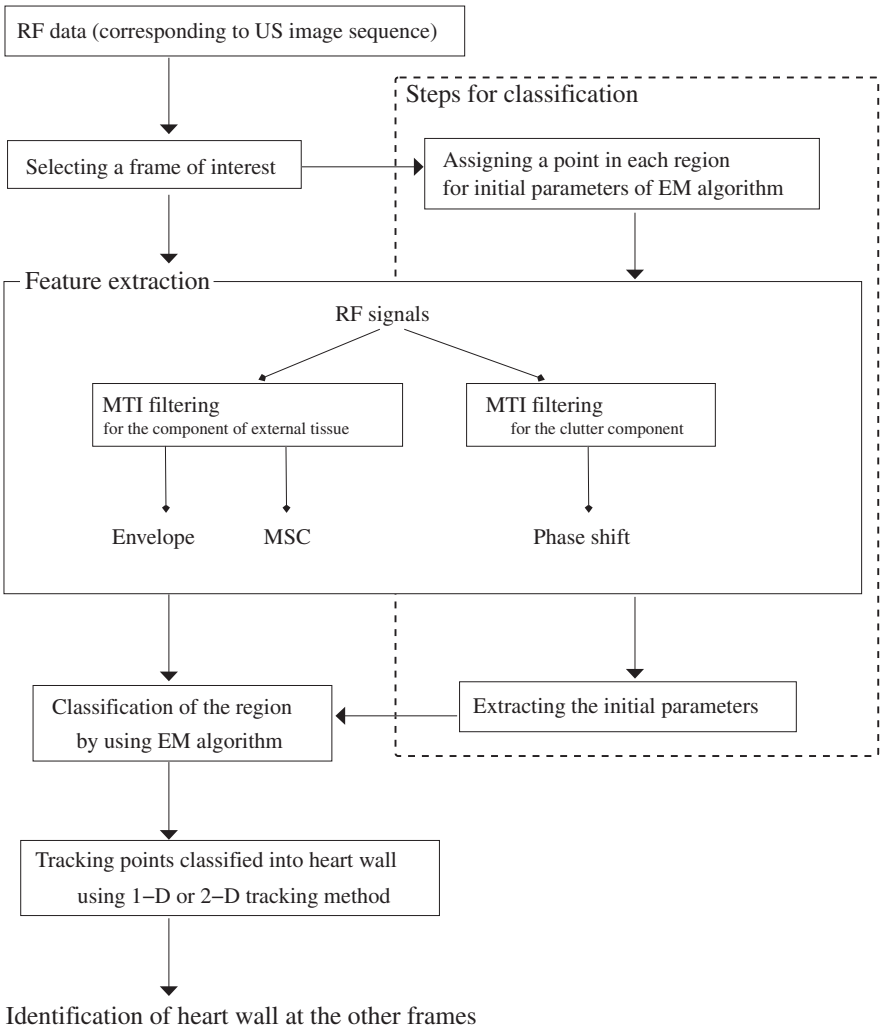

Fig. 4. Schematic procedure of identification of the heart wall proposed in this study.

respect to the direction of the frame to RF echoes from the position of the RV in each frame, which was acquired at a frame rate of 751 Hz and contained many of the echo components from the ribs. The displacement of each discrete point to be analyzed by DFT was tracked using the *phased tracking method*. As shown in Fig. 3(b), RF echoes in the RV mainly have components of approximately 0 Hz (stationary). It is necessary to reduce the components of the heart wall by MTI filtering as little as possible. Therefore, in this study, the cutoff frequency f_{c1} for the first and second features of the high-pass filter was set to 10 Hz (approximately 0 Hz).

On the other hand, for extracting the phase shift of echoes caused by blood flow in the lumen using the third feature $|\Delta\theta(i,j)|$, clutter components, which are signals scattered from slowly moving tissues except for blood cells, such as ribs and cardiac muscle, need to be reduced in the received RF signal. Therefore, the cutoff frequency, f_{c2}, of the MTI filter for the third feature has to be changed by referring to the velocity of cardiac muscle for extracting only the echoes from blood particles. In this study, the optimal cardiac phase was examined for various values of f_{c2}.

2.3 Classification method

Kinugawa *et al.* identified the heart wall on the basis of Bayes decision rule using probability distributions of the MSC of echoes from the heart wall and lumen, which had been manually segmented.[17] However, the parameters, used in the method, of probability distributions could not consider features of the other points except regions manually segmented. In this study, an expectation–maximization (EM) algorithm[27] for a mixture of Gaussian distributions was used to classify feature vectors, which were obtained from RF signals in a frame of interest, into either the heart wall or the lumen. Using the EM algorithm, parameters of the probability distribution, which better fits features of all points, are estimated. The probability distribution $P(\boldsymbol{d}_{i,j})$ of a feature vector $\boldsymbol{d}_{i,j}$, which is obtained from either of 2 classes, can be represented using a mixture of two Gaussian distributions as follows:

$$P(\boldsymbol{d}_{i,j}) = \pi_0 g(\boldsymbol{d}_{i,j}|\boldsymbol{\mu}_0, \boldsymbol{\Sigma}_0) + \pi_1 g(\boldsymbol{d}_{i,j}|\boldsymbol{\mu}_1, \boldsymbol{\Sigma}_1), \quad (5)$$

where $\{\pi_h\}$, $\{\boldsymbol{\mu}_h\}$, $\{\boldsymbol{\Sigma}_h\}$, and $g(\cdot)$ denote mixing coefficients, mean vectors, covariance matrices [lumen ($h = 0$) and heart wall ($h = 1$)], and Gaussian distribution, respectively. These parameters $\{\pi_h\}$, $\{\boldsymbol{\mu}_h\}$, and $\{\boldsymbol{\Sigma}_h\}$, which maximize the likelihood for a mixture of Gaussian distributions shown in eq. (5), can be estimated using an EM algorithm, one of the iterative calculation methods, based on extracted feature vectors. In this study, the initial parameters for the EM

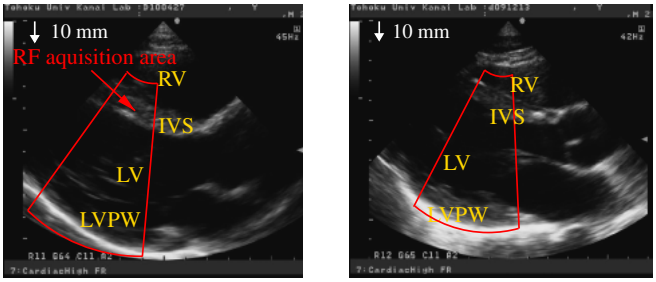

(a) (b)

Fig. 5. (Color online) Cross-sectional images of the left ventricle in longitudinal axis view obtained by conventional echocadiography for subjects (a) A and (b) B. The regions surrounded by a red line show acquisition areas of RF data.

algorithm were obtained using feature vectors extracted from the area around the point manually assigned in each region of a frame of interest. Using the estimated parameters, the posterior probability, $\nu(i,j)$, of the heart wall at each discrete point (i,j) is estimated as follows:

$$\nu(i,j) = \frac{\pi_1 g(\boldsymbol{d}_{i,j}|\boldsymbol{\mu}_1, \boldsymbol{\Sigma}_1)}{\pi_0 g(\boldsymbol{d}_{i,j}|\boldsymbol{\mu}_0, \boldsymbol{\Sigma}_0) + \pi_1 g(\boldsymbol{d}_{i,j}|\boldsymbol{\mu}_1, \boldsymbol{\Sigma}_1)}. \quad (6)$$

In this study, discrete points were classified into the heart wall ($h = 1$) when $\nu(i,j)$ exceeded 0.5.

Figure 4 shows the above-mentioned procedure proposed in this study for automated identification of the heart wall during an entire cardiac cycle. In the proposed method, selection of a frame of interest, i.e., the frame for the determination of regions to be tracked, is important because it affects the results of the identification of the heart wall in all following frames. Kinugawa *et al.* showed the results of identification of the heart wall based on the MSC in several cardiac phases.[17] However, the separability of the feature, MSC, in each cardiac phase was not evaluated. To accurately identify the heart wall in a frame of interest, in the present study, we investigated the optimal cardiac phase for classification as described below.

3. Evaluation of Separability in Each Cardiac Phase

3.1 High frame rate acquisition of RF signals

To accurately differentiate the heart wall from the lumen using features that are needed to estimate phase shift, it is essential that RF echo signals be measured at a high frame rate for the prevention of aliasing in the *phased tracking method*. To do that, the number of transmits, which is required to obtain the same number of scan lines as that in conventional sector scanning, was reduced by creating many focused receiving beams in one unfocused transmitting beam such as a plane wave [parallel beamforming (PBF)].[28,29]

3.2 Evaluation of separability

Figures 5(a) and 5(b) show acquisition areas of RF echoes in the longitudinal axis view of the hearts of two healthy 23-year-old males (subjects A and B) using a 3.75 MHz sector-type probe. Using PBF with plane wave transmission, the high frame rate (1010 Hz) measurement of RF echo data was realized with 80 scan lines with intervals of 0.375°. The

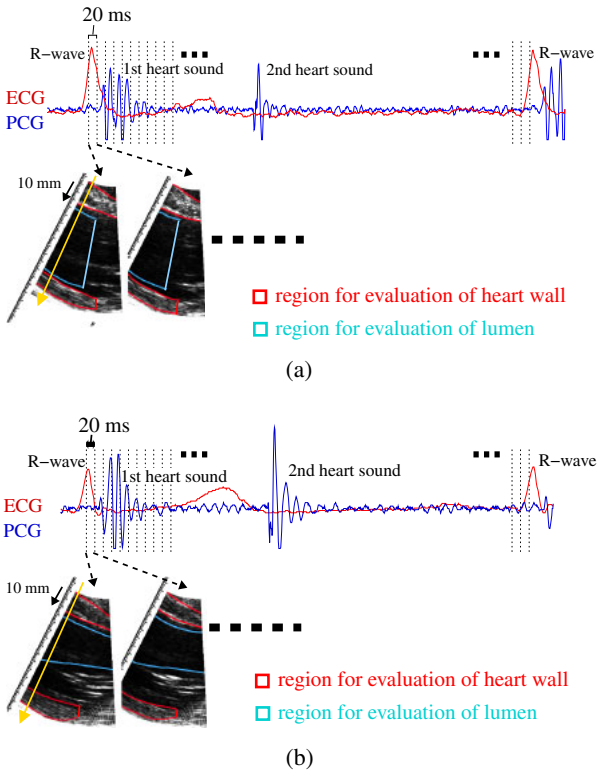

Fig. 6. (Color online) Regions manually assigned for evaluation of separability between heart wall and lumen for subjects (a) A and (b) B. Heart walls (IVS and LVPW) and lumen (LV) are shown as the areas surrounded by red and blue lines, respectively.

sampling frequency of the measured RF signals was 15 MHz. Using the three-dimensional feature vector variable $\boldsymbol{d}_{i,j} = (Env(i,j), |\gamma(i,j)|^2, |\Delta\theta(i,j)|)$ extracted at each discrete point in the acquisition areas, prior probabilities $\{p_h\}$, mean vectors $\{\boldsymbol{\mu}_h\}$, and covariance matrices $\{\boldsymbol{\Sigma}_h\}$ are calculated for classes $\{\omega_h\}$ [lumen ($h = 0$) and the heart wall ($h = 1$)] as follows:

$$p_h = \frac{N_h}{N} \quad (h \in \{0,1\}), \quad (7)$$

$$\boldsymbol{\mu}_h = \mathrm{E}_{i,j}[\boldsymbol{d}_{i,j}|\omega_h] \quad (h \in \{0,1\}), \quad (8)$$

$$\boldsymbol{\Sigma}_h = \mathrm{E}_{i,j}[(\boldsymbol{d}_{i,j} - \boldsymbol{\mu}_h)(\boldsymbol{d}_{i,j} - \boldsymbol{\mu}_h)^{\mathrm{T}}|\omega_h] \quad (h \in \{0,1\}), \quad (9)$$

$$\boldsymbol{\mu} = \sum_{h=0}^{1} p_h \mathrm{E}_{i,j}[\boldsymbol{d}_{i,j}|\omega_h], \quad (10)$$

where $\mathrm{E}_{i,j}[\cdot]$ denotes the spatial averaging in the axial and lateral directions, and N_h, N, and $\boldsymbol{\mu}$ are the number of feature vectors in each class, the total number of vectors in the area for evaluation, and the mean vector in all classes, respectively. As shown in Figs. 6(a) and 6(b), the class ω_h, to which each feature vector $\boldsymbol{d}_{i,j}$ belongs, was denoted by manually assigning areas in the heart wall and lumen, i.e., the IVS, LVPW, and LV, at intervals of 20 ms from the R-wave to the next R-wave. To evaluate the separability of the feature vector, the inter-class covariance matrix $\boldsymbol{S}_B$ in eq. (11), which corresponds to the distance between mean vectors of classes, and the intra-class covariance matrix $\boldsymbol{S}_W$ in eq. (12), which corresponds to the mean of the variances of feature vectors within classes, were defined using these parameters as follows:

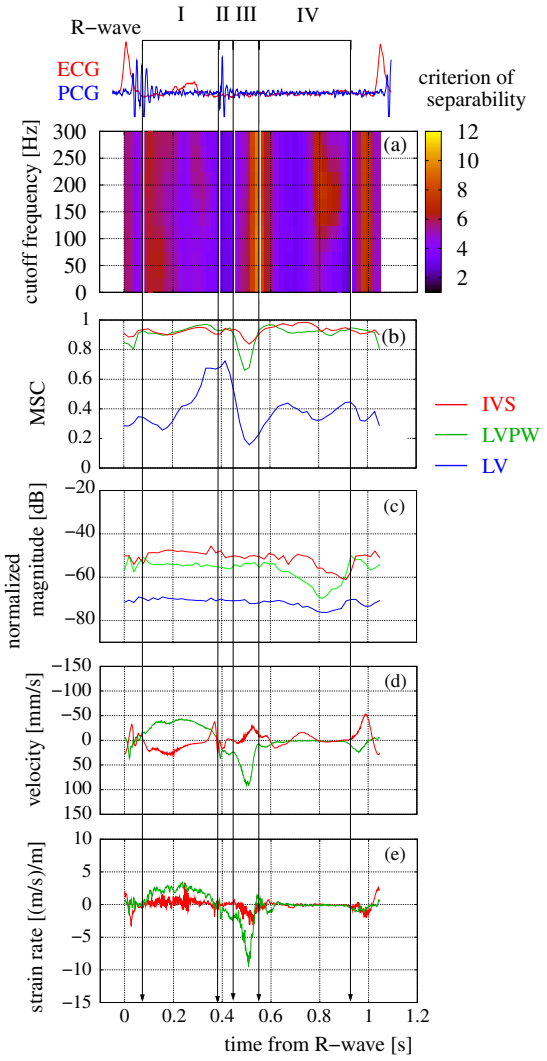

Fig. 7. (Color online) Results of subject A: (a) Criterion of separability J. Spatial means of (b) the MSC and (c) the envelope in each region manually assigned. (d) Velocities and (e) strain rate in IVS and LVPW on the beam shown by the yellow line in Fig. 6(a).

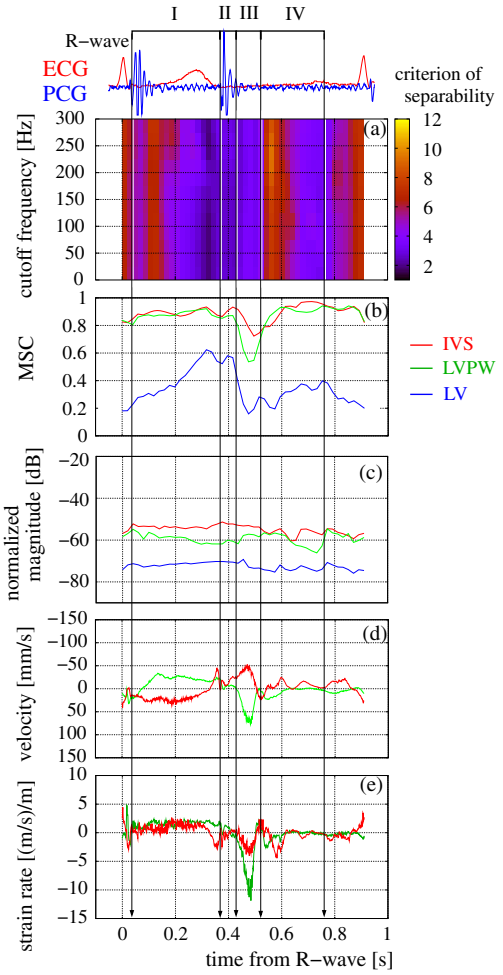

Fig. 8. (Color online) Results of subject B: (a) Criterion of separability J. Spatial means of (b) the MSC and (c) the envelope in each region manually assigned. (d) Velocities and (e) strain rate in IVS and LVPW on the beam shown by the yellow line in Fig. 6(b).

$$\boldsymbol{S}_B = \sum_{h=0}^{1} p_h(\boldsymbol{\mu}_h - \boldsymbol{\mu})(\boldsymbol{\mu}_h - \boldsymbol{\mu})^{\mathrm{T}}, \tag{11}$$

$$\boldsymbol{S}_W = \sum_{h=0}^{1} p_h \boldsymbol{\Sigma}_h, \tag{12}$$

The separability of the feature vector is increased in proportion to the distance between mean vectors of classes, whereas it is decreased in proportion to the variances of the vectors within classes.[30] Therefore, the criterion of separability J is defined by normalizing the inter-class covariance matrix $\boldsymbol{S}_B$ by the intra-class covariance matrix $\boldsymbol{S}_W$ as follows:[31]

$$J = \mathrm{tr}[\boldsymbol{S}_W^{-1}\boldsymbol{S}_B], \tag{13}$$

where tr[·] represents the sum of diagonal components. Figure 7(a) shows the criterion of separability, J, of subject A estimated using different values of f_{c2} of MTI filtering for the third feature. The spatial means of the envelope $Env(i,j)$ and the MSC $|\gamma(i,j)|^2$ in each frame, which correspond to the components of $\boldsymbol{\mu}_h$ in eq. (8), of subject A are shown in Figs. 7(b) and 7(c). In addition, Figs. 7(d) and 7(e) show velocities and strain rates in the axial direction of IVS and LV estimated by the *phased tracking method*[8,20] along the scan line shown by the yellow line in Fig. 6(a). Similarly, these values of subject B are shown in Figs. 8(a)–8(e). Periods I, II, III, and IV denote the ejection phase, isovolumic relaxation phase, rapid filling phase, and slow filling phase in Figs. 7 and 8.

3.3 Discussion of determination of optimal cardiac phase to select a frame of interest

As shown in both Figs. 7(a) and 8(a), results of subject A and subject B, the maximal values of J are found in the transition period, which is approximately 100 ms from the rapid filling phase (III) to the slow filling phase (IV). As shown in Figs. 7(b) and 8(b), this period shows greater separability owing to the large difference in the MSC between the heart wall region and the lumen region. The MSC in the lumen in this period is small because the blood velocity is high just after the rapid filling phase. Moreover, the MSC in the heart wall in this period is large because the strain rate of the cardiac muscle, which is a deformation of tissue changing the spacing of scatters,[32] is low, as shown in Fig. 7(e). The decrease in the strain rate of cardiac muscle in

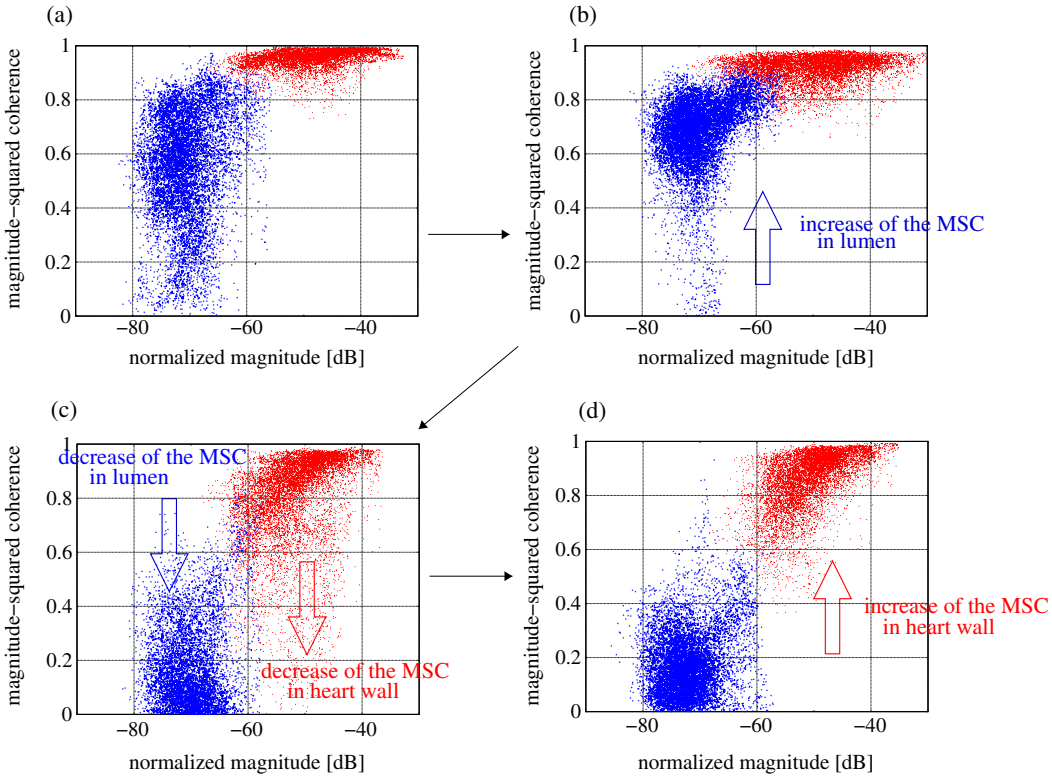

Fig. 9. (Color online) Distributions on two-dimensional feature space constructed by the first and second features, i.e., the envelope and the MSC, at each frame in (a) late ejection phase, (b) isovolumic phase, (c) rapid filling phase, and (d) the transition period from the rapid filling phase to the slow filling phase for subject A.

this period is found because the rapid extension of LV,[33] which corresponds to the increase in volume of LV, nearly finishes at the end of the rapid filling phase. Therefore, the transition period from the rapid filling phase to the slow filling phase is the valid cardiac phase to select a frame of interest in this study. As described above, the rapid filling phase is not suitable for the selection of a frame of interest because the MSC in the heart wall is lower owing to an increase in the strain rate of cardiac muscle accompanied by rapid extension of LV. From the late ejection phase to the isovolumic relaxation phase, the separability is low owing to an increase in the MSC in the lumen. Scatterers (blood cells) are likely to remain in an ultrasonic beam between two consecutive frames because the blood flow velocity is low in these cardiac phases. Tanaka *et al.* showed that the magnitude of the velocity vector of blood flow is about 20 cm/s and increased slightly to 50–60 cm/s at the aortic orifice in late systole.[34] The width of the emitted plane wave of PBF is 1.6 mm,[6] and blood cells may completely slip off from the beam during a period of about 3 to 8 ms in these cardiac phases under this condition. Therefore, these cardiac phases, when the blood flow velocity is decreased, are considered to show low separability due to a high temporal resolution of about 1 ms. The above-mentioned changes in the MSC appear as distributions of feature vectors in the feature space shown in Fig. 9.

For evaluation of the effect of the change in values of f_{c2}, the criterion of separability, J_3, of the third feature, $|\Delta\theta(i,j)|$, is obtained by normalizing the distance between means of classes by the variances of the third feature within classes, as well as by eq. (13), as follows:

$$J_3 = \frac{\sum_{h=0}^{1} p_h(\mu_{3h} - \mu_3)^2}{\sum_{h=0}^{1} p_h \mathrm{E}_{i,j}[(|\Delta\theta(i,j)| - \mu_{3h})^2|\omega_h]}, \qquad (14)$$

where μ_{3h} and μ_3 are the third component of $\boldsymbol{\mu}_h$ in eq. (8) and $\boldsymbol{\mu}$ in eq. (10), respectively. Figures 10(a) and 10(b) show the criterion of separability, J_3, of respective subjects estimated using different values of f_{c2} of MTI filtering, as in Figs. 7(a) and 8(a). The separability J_3 in each cardiac phase is changed by the value of cutoff frequency f_{c2}. In this study, the cutoff frequency f_{c2} was set to 200 Hz in the optimal cardiac phase, the transition period from the rapid filling phase to the slow filling phase, because the separability, J_3, of the third feature in this period was found to be high in the range of the cutoff frequency f_{c2} from 200 to 300 Hz.

4. Identification of Heart Wall Throughout Entire Cardiac Cycle

Figures 11(a) and 12(a) show B-mode and region-identified images in frames of interest selected in the transition period from the rapid filling phase to the slow filling phase for subjects A and B. The initial parameters of the EM algorithm were calculated by extracting feature vectors from the manually assigned regions, which are surrounded by the red line (heart wall) and the blue line (lumen) in Figs. 11(a) and 12(a). As shown in Figs. 11(a) and 12(a), the heart wall region was accurately identified in the frame of interest in the optimal cardiac phase. The heart wall in each frame throughout the entire cardiac cycle was identified by

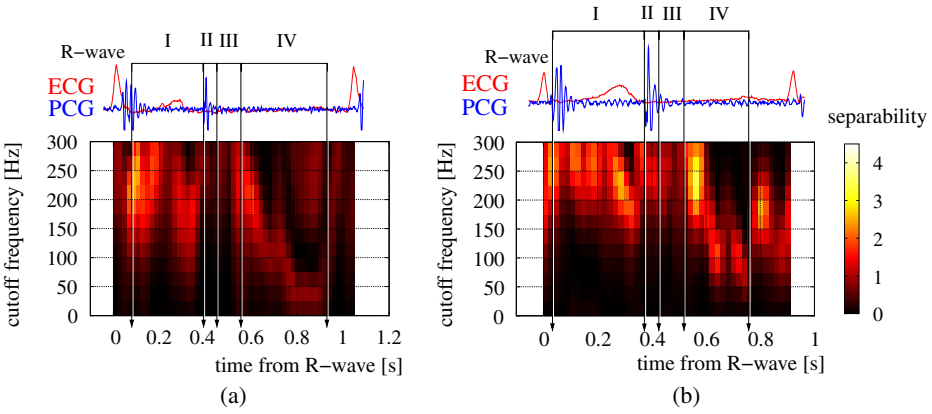

Fig. 10. (Color online) Criterion of separability J_3 of the third feature obtained with different values of cutoff frequency f_{c2} of MTI filtering for subjects (a) A and (b) B.

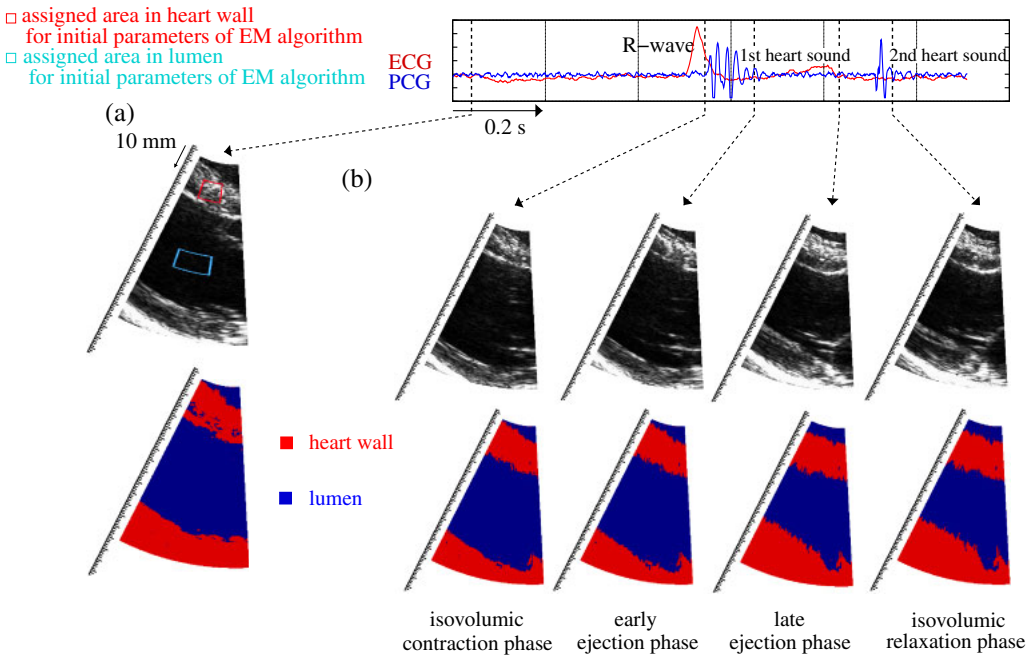

Fig. 11. (Color online) (a) B-mode and region-identified images in the frame of interest in the optimal cardiac phase for subject A. (b) Region-identified images obtained by tracking the points, which were classified as heart wall in the frame of interest, in the frame in isovolumic contraction phase (just after R-wave), in the early ejection phase, in the late ejection phase, and in the isovolumic relaxation phase.

tracking the points identified as the heart wall region in the frame of interest in Figs. 11(a) and 12(a) using the *phased tracking method*, as illustrated in Fig. 4. Figures 11(b) and 12(b) show region-identified images in the frames in different cardiac phases, i.e., the period just after the R-wave, early ejection phase, late ejection phase, and isovolumic relaxation phase, using the *phased tracking method*. The obtained results show that the method proposed in this study can identify the heart wall region during an entire cardiac cycle.

A serrated heart wall region is shown in Figs. 11(b) and 12(b). It was caused by difficulty in tracking points in the lumen around the boundary between the heart wall and lumen misclassified as the heart wall in the frame of interest. Therefore, a method for recovering the shape[14] of the heart wall in a frame of interest (or the following frames) should be further investigated. Moreover, further investigation is required for improving the separability of the proposed method, such as application of the 2D tracking method and a more effective classification method (e.g., changing the probability distribution for the EM algorithm), and improvement of MTI filtering.

5. Conclusions

In this study, we proposed a method for automated identification of the heart wall region throughout an entire cardiac cycle and determined the optimal cardiac phase to select a frame of interest, i.e., a frame for the initiation of tracking. To determine the optimal cardiac phase, the separability of classes was quantitatively evaluated in each cardiac phase for two subjects. The heart wall was accurately identified in a frame of interest in the optimal cardiac phase

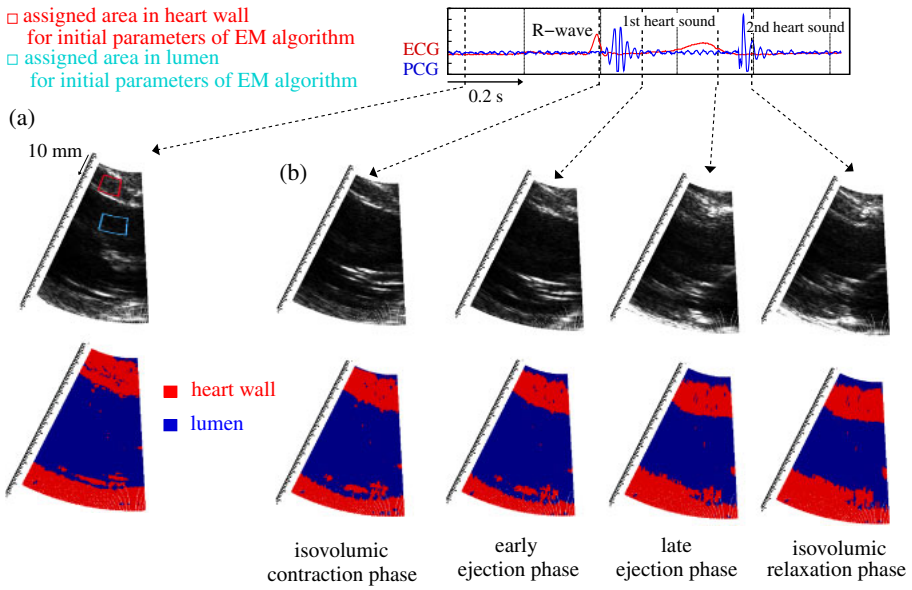

Fig. 12. (Color online) (a) B-mode and region-identified images in the frame of interest in the optimal cardiac phase for subject B. (b) Region-identified images obtained by tracking the points, which were classified as heart wall in the frame of interest, in the frame in isovolumic contraction phase (just after R-wave), in the early ejection phase, in the late ejection phase, and in the isovolumic relaxation phase.

by applying the EM algorithm, i.e., one of the classification methods, to extracted feature vectors, and heart wall regions in the following frames were also identified by tracking each point classified as the heart wall region using the *phased tracking method*. The results indicate the feasibility of the proposed method in the longitudinal axis view. To apply the proposed method to ultrasonic images in various cardiac views, the optimal cardiac phase should be further investigated in the short axis and apical views of the heart.

1) G. R. Sutherland, G. D. Salvo, P. Claus, J. D'hooge, and B. Bijnens: J. Am. Soc. Echocardiogr. **17** (2004) 788.
2) W. N. McDicken, G. R. Sutherland, C. M. Moran, and L. N. Gordon: Ultrasound Med. Biol. **18** (1992) 651.
3) L. N. Bohs, B. J. Geinman, M. E. Anderson, S. C. Gebhart, and G. E. Trahey: Ultrasonics **38** (2000) 369.
4) K. Kaluzynski, X. Chen, S. Y. Emelianov, A. R. Skovoroda, and M. O'Donnell: IEEE Trans. Ultrason. Ferroelectr. Freq. Control **48** (2001) 1111.
5) J. D'hooge, E. Konofagou, F. Jamal, A. Heimdal, L. Barrios, B. Bijnens, J. Theoen, F. V. de Werf, G. R. Sutherland, and P. Suetens: IEEE Trans. Ultrason. Ferroelectr. Freq. Control **49** (2002) 281.
6) Y. Honjo, H. Hasegawa, and H. Kanai: Jpn. J. Appl. Phys. **49** (2010) 07HF14.
7) H. Kanai: IEEE Trans. Ultrason. Ferroelectr. Freq. Control **52** (2005) 1931.
8) H. Yoshiara, H. Hasegawa, H. Kanai, and M. Tanaka: Jpn. J. Appl. Phys. **46** (2007) 4889.
9) H. Kanai: Ultrasoud Med. Biol. **35** (2009) 936.
10) V. Chalana and Y. Kim: IEEE Trans. Med. Imaging **16** (1997) 642.
11) E. Brandt, L. Wigström, and B. Wranne: Proc. MICCI'99, 1999, p. 410.
12) Q. Duan, E. D. Angelini, S. L. Herz, C. M. Ingrassia, K. D. Costa, J. W. Holmes, S. Homma, and A. F. Laine: Ultrasound Med. Biol. **35** (2009) 256.
13) M. Papadogiorgaki, V. Mezaris, Y. S. Chatzizisis, G. D. Giannoglou, and I. Kompatsiaris: Ultrasound Med. Biol. **34** (2008) 1482.
14) C. Y. Chang, Y. F. Lei, C. H. Tseng, and S. R. Shih: IEEE Trans. Biomed. Eng. **57** (2010) 1348.
15) A. H. Torp, S. I. Rabben, A. Støylen, H. Ihlen, K. Anderson, L. Å. Brodin, and B. Olstad: Proc. 2004 IEEE Ultrasonics Symp., 2004, p. 474.
16) M. M. Nillesen, R. G. P. Lopata, I. H. Gerrits, L. Kapusta, H. J. Huisman, J. M. Thussen, and C. L. D. Korte: Ultrasoud Med. Biol. **33** (2007) 1453.
17) T. Kinugawa, H. Hasegawa, and H. Kanai: Jpn. J. Appl. Phys. **47** (2008) 4155.
18) B. Hete and K. K. Shung: IEEE Trans. Ultrason. Ferroelectr. Freq. Control **40** (1993) 354.
19) S. A. Wickline, L. J. Thomas III, J. G. Miller, B. E. Sobel, and J. E. Perez: J. Clin. Invest. **76** (1985) 2151.
20) H. Kanai, M. Sato, Y. Koiwa, and N. Chubachi: IEEE Trans. Ultrason. Ferroelectr. Freq. Control **43** (1996) 791.
21) H. Takahashi, H. Hasegawa, and H. Kanai: Cho-onpa Igaku **36** (2009) 679 [in Japanese].
22) C. Kasai, K. Namekawa, A. Koyano, and R. Omoto: IEEE Trans. Sonics Ultrason. **32** (1985) 458.
23) L. Hatle and B. Angelsen: *Doppler Ultrasound in Cardiology* (Lea & Febiger, St. Louis, MO, 1982) 2nd ed.
24) L. Kapusta, J. M. Thussen, M. H. M. Cuypers, P. G. M. Peer, and O. Daniëls: Ultrasoud Med. Biol. **26** (2000) 229.
25) T. Higuchi and M. Kawamata: *Digital Shingoshori—MATLAB Taio—* (Digital Signal Processing: With MATLAB Exercises) (Shokodo, Tokyo, 2000) [in Japanese].
26) B. R. Mahafza: *Introduction to Rader Analysis* (CRC Press, Boca Raton, FL, 1998).
27) A. P. Dempster, N. M. Laird, and D. B. Rubin: J. R. Stat. Soc., Ser. B **39** (1977) 1.
28) M. Tanter, J. Bercoff, L. Sandrin, and M. Fink: IEEE Trans. Ultrason. Ferroelectr. Freq. Control **49** (2002) 1363.
29) H. Hasegawa and H. Kanai: IEEE Trans. Ultrason. Ferroelectr. Freq. Control **55** (2008) 2626.
30) C. M. Bishop: *Pattern Recognition and Machine Learning* (Springer, Berlin, 2006).
31) K. Fukunaga: *Introduction to Statistical Pattern Recognition* (Academic Press, San Diego, CA, 1990) 2nd ed.
32) H. Hasegawa and H. Kanai: IEEE Trans. Ultrason. Ferroelectr. Freq. Control **55** (2008) 1921.
33) A. M. Katz: *Physiology of the Heart* (Lippincott Williams & Wilkins, Philadelphia, PA, 2001).
34) M. Tanaka, T. Sakamoto, S. Sugawara, H. Nakajima, Y. Katahira, S. Ohtsuki, and H. Kanai: J. Cardiol. **52** (2008) 86.